

Palaeomagnetism in the Sines massif (SW Iberia) revisited: evidences for Late Cretaceous hydrothermal alteration and associated partial remagnetization

P. Ribeiro,^{1,2} P. F. Silva,^{3,4} P. Moita,⁵ Z. Kratinová,⁶ F. O. Marques⁷ and B. Henry⁸

¹*Centro de Geofísica da Universidade de Coimbra (CGUC), Av. Dr. Dias da Silva, 3000-134 Coimbra, Portugal. E-mail: pribeiro@ci.uc.pt*

²*Observatório Geofísico e Astronómico da Universidade de Coimbra, Av. Dr. Dias da Silva, 3000-134 Coimbra, Portugal*

³*Instituto Superior de Engenharia de Lisboa (ISEL/ADF), Rua Conselheiro Emídio Navarro, 1, 1959-007 Lisboa, Portugal*

⁴*Instituto Dom Luiz, Universidade de Lisboa, Campo Grande, Edifício C8, Piso 3, 1749-016 Lisboa, Portugal*

⁵*Centro de Geofísica de Évora, Universidade de Évora, Rua Romão Ramalho, 59, 7000 Évora, Portugal*

⁶*Institute of Geophysics ASCR, v.v.i., Prague, Czech Republic*

⁷*Universidade de Lisboa, Alameda da Universidade, 1649-004 Lisboa, Portugal*

⁸*Paléomagnétisme, Institut de Physique du Globe de Paris, Sorbonne Paris Cité, Univ Paris Diderot, and UMR 7154 CNRS, France*

Accepted 2013 July 2. Received 2013 June 19; in original form 2012 November 5

SUMMARY

This study revisits the palaeomagnetism of the Sines massif (~76 Ma) in the southwestern Iberian Margin (Portugal). The palaeomagnetic analysis was complemented by a comprehensive study of the magnetic mineralogy by means of rock magnetic measurements and petrographic observations. The overall dispersion of palaeomagnetic directions (declination ranging between ~N0° and ~N50°) and their migration observed during stepwise demagnetizations have revealed the superposition of remanence components. We interpret this complex palaeomagnetic behaviour as related to the regional hydrothermalism associated with the last stages of Late Cretaceous magmatic activity. This environment favoured mineralogical alteration and a partial chemical remagnetization, giving in most samples a composite magnetization, which has been erroneously interpreted as the primary one in a previous study, then leading to a questionable model for Cretaceous Iberia rotation. Nonetheless, for some samples a single component has been isolated. Interesting rock magnetic properties and microscopic observations point to a well-preserved magnetic mineralogy for these samples, with magnetite clearly of primary origin. The associated ChRM mean direction ($D/I = 3.9^\circ/46.5^\circ$, $\alpha_{95} = 1.7^\circ$, $N = 31$ samples) then represents the true primary magnetization of the Sines massif. This new palaeomagnetic direction and the corresponding palaeomagnetic pole (long = 332.0°, lat = -79.5°, $A_{95} = 1.7^\circ$) agrees with those from the other palaeomagnetic works for the same period and region (e.g. the Sintra and Monchique massifs), yielding a lack of significant rotation of Iberia relative to stable Europe since the uppermost Late Cretaceous (Campanian–Maastriichtian).

Key words: Magnetic fabrics and anisotropy; Magnetic mineralogy and petrology; Palaeomagnetism applied to tectonics; Remagnetization.

1 INTRODUCTION

The opening of Biscay Bay and consequent counter-clockwise rotation of Iberia with respect to Eurasia is a long-standing geodynamic problem (Argand 1924; Du Toit 1937; Carey 1958; Bullard *et al.* 1965). In the following years, numerous marine geological and geophysical studies confirmed the Argand's hypothesis by showing the oceanic nature with linear magnetic anomalies of the Biscay Bay (Williams 1975; and references therein). Several kinematic models have been then proposed for the opening of the Biscay Bay, the rotation of Iberia and its relation to the formation of Pyrenees (e.g.

Srivastava *et al.* 1990; Sibuet & Collette 1991; Olivet 1996; 2000; Sibuet *et al.* 2004; Vissers & Meijer 2012).

The Iberian rotation puzzle was also addressed by palaeomagnetists since the early 1960s (Schwarz 1963; Girdler 1965; Van der Voo 1967; Van Dongen 1967; Watkins & Richardson 1968). The comprehensive work of Van der Voo (1969) provided the strongest support for the Argand's hypothesis using the palaeomagnetic results obtained from rocks of different ages from Portugal and Spain. It concluded that Iberia rotated of approximately 35° anticlockwise between the Late Triassic and the Late Cretaceous. Later, the palaeomagnetic directions of the Iberian rocks have been investigated to

Table 1. Selected palaeomagnetic results (ChRMs directions) of the Late Cretaceous igneous rocks from Portugal; D, declination; I, inclination; N, number; α_{95} , confidence limit.

Site (locality)	Age (Ma)	D (°)	I (°)	N	α_{95} (°)	Reference
Foz da Fonte (Sesimbra)	~94	346.5	44.3	73	3.1	Neres <i>et al.</i> (2012)
Paço d'Ilhas (Ribamar)	~88	350	42.2	275	1.4	Neres <i>et al.</i> (2012)
		359	43.5	25	5.0	Van der Voo (1969)
Sintra complex	~83–80	358	27.3	34	3.3	Storetvedt <i>et al.</i> (1987)
Sines complex	~76	40.8	41.4	36	3.3	Storetvedt <i>et al.</i> (1987)
Lisbon volcanic complex	~72	352	40	33	3.0	Van der Voo & Zijdeveld (1971)
Monchique complex	~70	182	−37	8	6.5	Van der Voo (1969)
		181	−42	27	4.5	Storetvedt <i>et al.</i> (1990)

better constrain the Iberian rotation (e.g. Van der Voo & Zijdeveld 1971; Storetvedt 1973; Vandenberg 1980; Storetvedt *et al.* 1987, 1990; Galdeano *et al.* 1989; Moreau *et al.* 1992, 1997; Dinarés-Turell & Garcia-Senz 2000; Márton *et al.* 2004; Gong *et al.* 2008; Osete *et al.* 2011; Neres *et al.* 2012; Ruiz-Martínez *et al.* 2012).

Various models of Iberia rotation were proposed based on palaeomagnetic studies. Among them, Storetvedt *et al.* (1987, 1990) proposed a two-phase rotation model mainly based on data obtained from the Sines massif (Portugal). According to these authors, Iberia experienced two consecutive rotations of opposite sense during the Late Cretaceous. This model was initially proposed to explain the northeasterly direction ($D = 40.8^\circ$, $I = 41.4^\circ$, $\alpha_{95} = 3.3^\circ$; *cf.* Table 1) obtained for the Late Cretaceous complex of Sines. Interpreted by these authors as a primary component, this northeasterly characteristic direction deviates significantly from the mean northerly directions reported for the other Portuguese Late Cretaceous alkaline complexes, namely the Sintra and Monchique (Table 1). Mainly due to its incompatibility with the kinematic models proposed on the basis of the seafloor magnetic anomalies (e.g. Srivastava *et al.* 1990; Sibuet *et al.* 2004; Vissers & Meijer 2012), this interpretation has been considered somewhat speculative and, therefore, generally rejected (Van der Voo 1993), but without actually reliable palaeomagnetic arguments. Therefore, a detailed analysis of the palaeomagnetic data of the Sines massif is of key importance for the models of Iberia rotation.

The aim of this study is reanalyse in detail the data from the Sines massif by a new and comprehensive palaeomagnetic study complemented by the rock magnetism, magnetic fabrics and microscopic studies. We intend to bring new insights into the geodynamic evolution and also in understanding of role of hydrothermal alteration for the interpretation of palaeomagnetic data.

2 GEOLOGICAL AND TECTONIC SETTING

The studied rocks of the Sines massif forms part of the 'Late Cretaceous Iberian Alkaline Province' (Macintyre & Berger 1982; Rock

1982) that is found in the West Iberia Margin, northern Spain and Pyrenees. The main Portuguese onshore occurrences comprise the Lisbon volcanic complex, and the Sintra, Sines and Monchique subvolcanic massifs.

Several isotopic studies have been conducted to constrain the timing and duration of alkaline cycle on the West Iberia Margin (e.g. Ferreira & Macedo 1979; Canilho & Abranches 1982; Storetvedt *et al.* 1987; Bernard-Griffiths *et al.* 1997). Miranda *et al.* (2009) and Grange *et al.* (2010) constrained the duration of the alkaline cycle to a period of approximately 25 Ma between ~94 and ~69 Ma based on U-Pb, $^{40}\text{Ar}/^{39}\text{Ar}$ and Rb-Sr ages of several intrusions exposed along the Portuguese coast. In addition, Miranda *et al.* (2009) recognized two pulses of magmatic activity: the first pulse was restricted to sills in the Lisbon region and occurred between 94 and 88 Ma, within the opening period of the Biscay Bay (118–80 Ma; Sibuet *et al.* 2004); the second one occurred in the approximate interval 75–72 Ma, corresponding to a more diversified mode of occurrence (subvolcanic complexes, lava flows, plugs, dykes and sills). Recently, the emplacement age of the Sines massif was obtained by means of the U-Pb method (on zircons and titanites) being 75.4 ± 0.6 Ma and 76.1 ± 1.3 Ma, respectively (Miranda *et al.* 2009; Grange *et al.* 2010; Table 2).

The Sines massif occurs halfway between the Sintra and Monchique massifs on the south Portuguese coast (SW Iberia, Fig. 1a). It is located on the southern limit of the Santiago do Cacém intracratonic basin, which was related to the rifting episodes that affected the West Iberian Margin during North Atlantic opening. This small basin is limited to the west by a major NNE–SSW fault (St André) that played an important role in tectonic and sedimentary evolution (Inverno *et al.* 1993, inset in Fig. 1b). On land, the Sines massif is relatively small (~10 km²) and, despite a large Plio-Quaternary cover (the major part of the outcrops are on the seacoast and in a large quarry), shows an apparent subvolcanic ring-structure (Teixeira 1962; Ribeiro *et al.* 1979). Using magnetic, gravimetric and seismic reflection data from offshore, Carvalho *et al.* (1998) were able to model a large igneous body (~300 km²) with an NE–SW global direction, and with its roof lying approximately at 600 m below the seafloor.

Table 2. Summary of the ages (with the respective uncertainties; $\pm 1\sigma$ Ma) obtained for the Sines massif by several authors using different isotopic techniques.

Reference	Method	Material	Age (Ma)
Mendes (1968)	Rb-Sr	Biotite and whole rock	72.1 ± 0.7
Canilho (1972)	K-Ar	Whole rock	72.8
Canilho & Abranches (1982)	Rb-Sr	Whole rock (isochron)	72.0 ± 1.5
Storetvedt <i>et al.</i> (1987)	K-Ar	Whole rock and k-feldspar	76.5 ± 2.0
Miranda <i>et al.</i> (2009)	U-Pb	Zircon	75.4 ± 0.6
Grange <i>et al.</i> (2010)	U-Pb	Zircon and titanite	76.1 ± 1.3

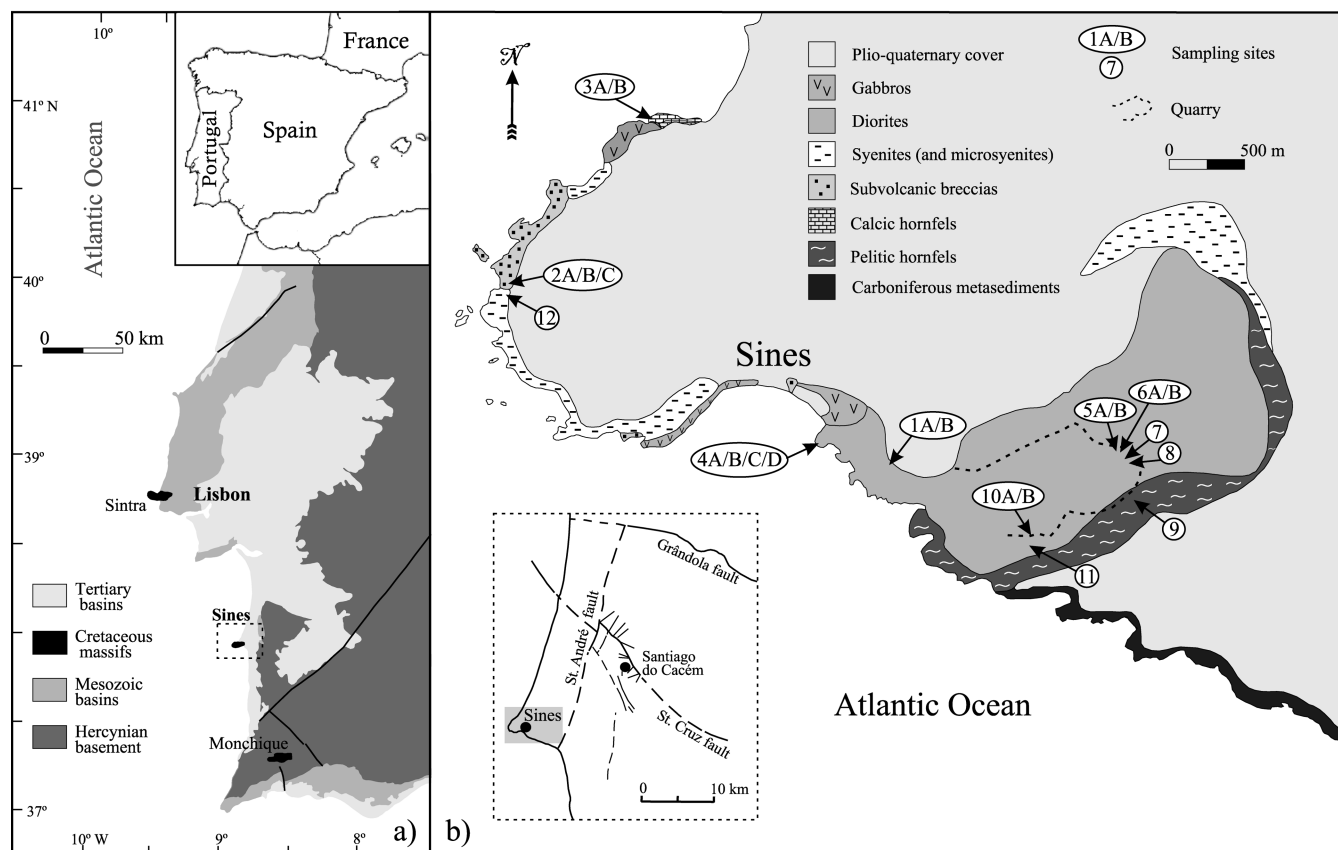


Figure 1. (a) Simplified geological map of Portugal showing the main Late Cretaceous alkaline massifs (Sintra, Sines and Monchique); (b) Geologic map of Sines (modified from Canilho 1972) with sampling localities.

The Sines massif intruded Carboniferous metasediments (schists and greywackes of the Mira Formation—South Portuguese Zone of Iberian Hercynian Segment) and Jurassic limestones. The intrusion generated relatively narrow thermal aureoles composed of fine-grained calcic hornfels at the northwest and pelitic hornfels at the southeast contacts (Fig. 1b).

The Sines subvolcanic massif is mainly formed by gabbros, diorites and syenites. The subordinate rock types (occurring mainly in dykes) are basalts, microgabbros, microdiorites, trachybasalts, lamprophyres, trachytes and microsyenites (Canilho 1972; Inverno *et al.* 1993). Canilho (1972, 1989) argued that these magmatic rocks originated in a common magmatic chamber by fractional crystallization. Mainly based on the structural relations, a multiphase model of the massif emplacement has been proposed (Zbyszewski 1941; Canilho 1972; Inverno *et al.* 1993). The emplacement started with the intrusion of gabbro-diorite mass, which was followed by the intrusion of syenitic rocks and the subsequent formation of eruptive breccias (with some basaltic masses). Finally, the entire massif and the surrounding country rocks were cut by a dense net of basic and acid subvertical dykes, with N–S and E–W prevailing trends.

3 SAMPLING AND METHODS

Standard palaeomagnetic samples were taken by a portable gasoline-powered drilling machine. 191 samples were oriented by means of both magnetic and sun compass in 12 stations (Fig. 1b). For some stations, different rock formations (lithologies) of the massif were sampled, each one here mentioned as site.

At station SI1, which corresponds to a fresh exposure near the local quarry, samples of gabbros (site SI1A) and a mafic dyke (site SI1B) were collected. At station SI2, three sites of different lithologies were sampled in coastal outcrops, comprising fine-grained felsic contorted dyke (site SI2A), fine-grained mafic dyke (SI2B) and ground mass of a rock formation, which has been mapped as a subvolcanic breccia (site SI2C). The station SI3 comprises calcic hornfels outcropping along the beach in the northern sector of massif (contact aureole). At station SI4, the diorite (SI4B) and three mafic dykes (SI4A, SI4C and SI4D) outcropping at south of Praia Grande were sampled. In the stations 5, 6, 7 and 8, closely spaced along the ground level of the ~N–S cutting wall of the quarry, samples of gabbros (SI5A and SI6A), mafic dykes (SI5B and SI6B) and metasedimentary enclaves (SI7 and SI8) were collected. Samples of siliceous hornfels belonging to the southern contact aureole were obtained at station SI9. At station SI10 (southern limit of quarry) were sampled the gabbro ground mass (SI10A) and another mafic dyke (SI10B). Close to this station, metasedimentary enclaves were drilled at station SI11. Syenite samples were obtained in the station SI12, near the contact with the subvolcanic breccia.

Thermal (TH) and alternating field (AF) demagnetizations were used to analyse the natural remanent magnetization (NRM) components. The latter were determined for each sample using linear segments on the Zijderveld diagrams (Kirschvink 1980). The site-mean direction associated with its angular confidence zone (α_{95}) and precision parameter (k) was determined following the Fisher statistics (Fisher 1953). Before the demagnetization procedures, the samples were maintained in zero magnetic field for a minimum

period of 1 month to reduce a potential Viscous Remanent Magnetization (VRM) effect.

The identification and characterization of physical properties of the main magnetic carriers is of principal importance in deciphering the nature and timing of acquired remanent magnetizations. In this study, a combination of rock magnetism, microscopic techniques and anisotropy of magnetic susceptibility (AMS) methods was applied in addition to the classical palaeomagnetic analyses to precisely characterize the palaeomagnetic record.

The measurements of magnetic susceptibility and remanence were done with an MFK1-FA Kappabridge and JR5, JR6A and 2G magnetometers, respectively. Thermomagnetic— $K(T)$ analyses were performed between -190 and 700 °C using a cryogenic attachment (CS-L) and a furnace (CS-4) coupled to the MFK1-FA. High-temperature runs were performed under an Argon-controlled atmosphere. At least one sample per site was analysed at low and high temperatures. Classical hysteresis curves were obtained on small samples (about 3 cm^3) using a laboratory-made translation inductometer within an electromagnet (Saint Maur, IPGP) up to a maximum applied field of 800 mT.

The magnetic susceptibility ellipsoid was characterized using Jelínek (1981) parameters (corrected degree of anisotropy— P' and shape parameter— T). AMS mean principal magnetic susceptibility axes, maximum ($K1$), intermediate ($K2$) and minimum ($K3$) that define the orientation of the magnetic ellipsoid were determined by tensor variability statistics (Hext 1963; Jelínek 1978). The aim was to check possible effects of magnetic fabric on the palaeomagnetic directions. The AMS was measured for all types of rock. In addition, detailed AMS studies of two dykes (SI4C and SI4D) were performed.

4 PALAEOMAGNETIC RESULTS

Pilot palaeomagnetic tests conducted for each site/lithology mostly reveal a coherent evolution of the directions during the demagnetization. The directional behaviours of samples from the sites SI2A (felsic dyke), SI3A (Ca-metasediments) and SI4A (mafic dyke) were erratic and consequently excluded for further studies (see example at Fig. 2a).

AF demagnetizations show a relatively fast decay of the remanence intensity, with 10 per cent of the signal typically remaining for fields above 30–50 mT (Fig. 2). That shows the soft nature of their magnetization, characteristic of low-coercivity magnetic phases. Thermal treatments reveal 580 °C as the maximum unblocking temperature, with 10–40 per cent cleaned up to 500 °C, while the remaining signal disappears either gradually up to the maximum unblocking temperature or more abruptly between 550 and 570 °C. The weak decrease of the remanent magnetization for the low temperature steps indicates the absence of significant VRM.

The evolution of the magnetization direction reflects different cases during demagnetization:

- Some samples show a linear (or quasi-linear) direction that remains stable until the last demagnetization steps (Figs 2b, h and m).
- However, the great majority of the samples shows a progressive evolution: mostly from NNE or NE declinations towards a northerly direction (Figs 2c–g and i), less frequently (only station SI4, in dykes and diorites) from the southeastern quadrant towards an NE declination (Figs 2j and k) and rarely in the opposite sense (Fig. 2l); the two main trajectories of the magnetization directions during demagnetization intersect at $D = 38.2^\circ$, $I = 38.5^\circ$, with

$\alpha_{95} = 2.2^\circ$ for $N = 39$ (Fig. 2n). For part of these samples, the best-fitting analyses retrieve a stable direction for the last demagnetization steps, commonly above temperatures (fields) of 560 °C (20 mT). For the remaining part, the curved shape persists on the Zijderveld diagram until the last demagnetization steps (even for thermal demagnetization performed with steps of 1° for the last 10–20 °C). These results indicate the presence of partial superposition of the unblocking temperature/field spectra, that is, a composite magnetization that forbids the determination of a reliable direction by principal component analysis.

For those samples, which reveal stable directions, the fitted line that defines the high-temperature component exactly crosses the axes origin of the Zijderveld diagram (ChRM) only for the directions around 0° in declination (Fig. 2n). That is not the case for the directions with a declination scattered between that of the ChRMs and 50° . For these last directions, it is clear that they result from the superposition of at least two components.

To summarize, in this work we are faced with a very complex palaeomagnetic signature resulting from multiple components. Therefore, it is necessary to proceed with a detailed study of the magnetic carriers to understand their origin and nature, the subject of the next two sections.

5 ROCK MAGNETISM

5.1 Bulk magnetic values

NRM and bulk magnetic susceptibility (K) results reveal a wide variation of intensities, ranging from 10^{-3} to 10^{+1} A m^{-1} and 10^{-4} to 10^{-1} SI , respectively. These values are positively correlated (Fig. 3a). The highest values of these magnetic parameters were mostly found for gabbros and subvolcanic breccias ($6\text{--}7\text{ A m}^{-1}$; $10\text{--}100 \times 10^{-3}\text{ SI}$) and the lowest ones ($<0.1\text{ A m}^{-1}$; $<1 \times 10^{-3}\text{ SI}$) for metasediments (calic and siliceous), mafic dykes and diorites. The corresponding Koenigsberger ratio mostly ranges between 0.1 and 8. Such results reflect variable magnetic mineral compositions and/or contents (e.g. Borradaile & Henry 1997; Borradaile & Jackson 2010), sometimes, even for the same lithology.

5.2 Thermomagnetic analysis

Different types of $K(T)$ cycles have been identified according to the rock type (Figs 3b and c). The Verwey transition (Verwey 1939) is mostly observed despite its signature varies according to the rock type. The gabbro, Ca-metasediments and subvolcanic breccia show a sharp transition for temperatures around -160 °C, pointing for the presence of stoichiometric magnetite. For mafic dykes, when observed, the Verwey transition is responsible for a smooth variation of the $K(T)$ curve around -160 °C. Above the Verwey transition, the $K(T)$ curves exhibit a paramagnetic hyperbolic decay up to 200–400 °C, particularly notable for diorites and mafic dykes, indicating a significant contribution of paramagnetic minerals for the susceptibility values.

The high-temperature $K(T)$ signature is also distinct according to the sites and rocks. In the case of gabbros, Ca-metasediments and subvolcanic breccias, $K(T)$ cycles are reversible and show an abrupt decay of $K(T)$ values above 560 °C, defining the Curie temperature around 580 °C. This behaviour is characteristic of magnetite (e.g. O'Reilly 1984; Petrovský & Kapička 2006), then in agreement with the indication given by the Verwey transition. On the other hand, $K(T)$ of diorite and mafic dykes show irreversible $K(T)$ curves where

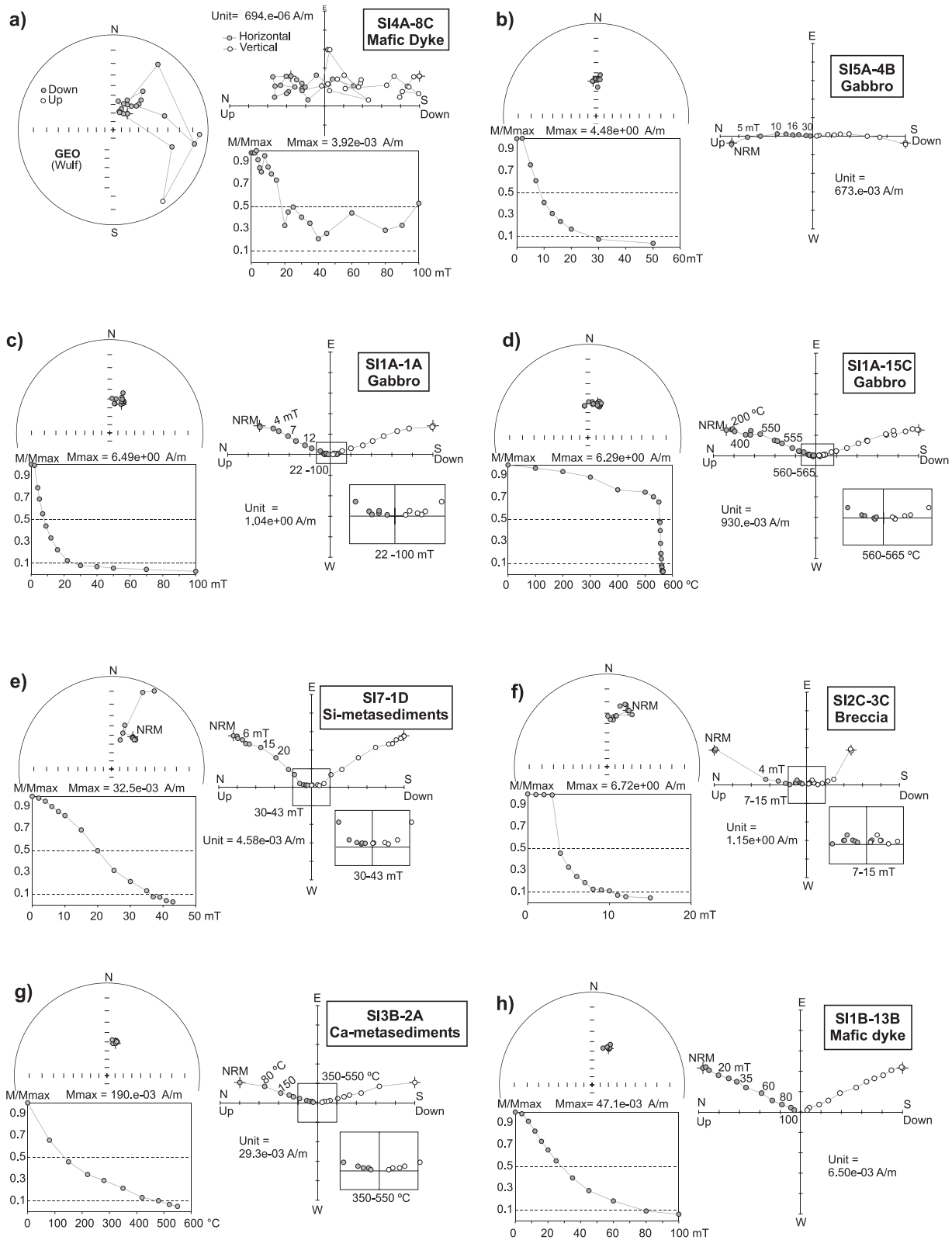


Figure 2. Representative examples (a–m) of the direction and intensity evolution of the NRM during alternating field (AF) and thermal demagnetization procedures (Zijderveld diagrams), and stereographic projections and remanence intensity decay curves; (n) Stereographic projections showing the observed great circle trajectories (left-hand side) and palaeomagnetic directions (right-hand side). On the Zijderveld diagram, solid (open) circles represent projection on the horizontal (vertical) plane; on the stereographic projection, solid (open) circles represent projection on the lower (upper) hemisphere; Solid lines on stereographic projections of samples (SI1A-12C and SI4B-11C) represent their great circle trajectories.

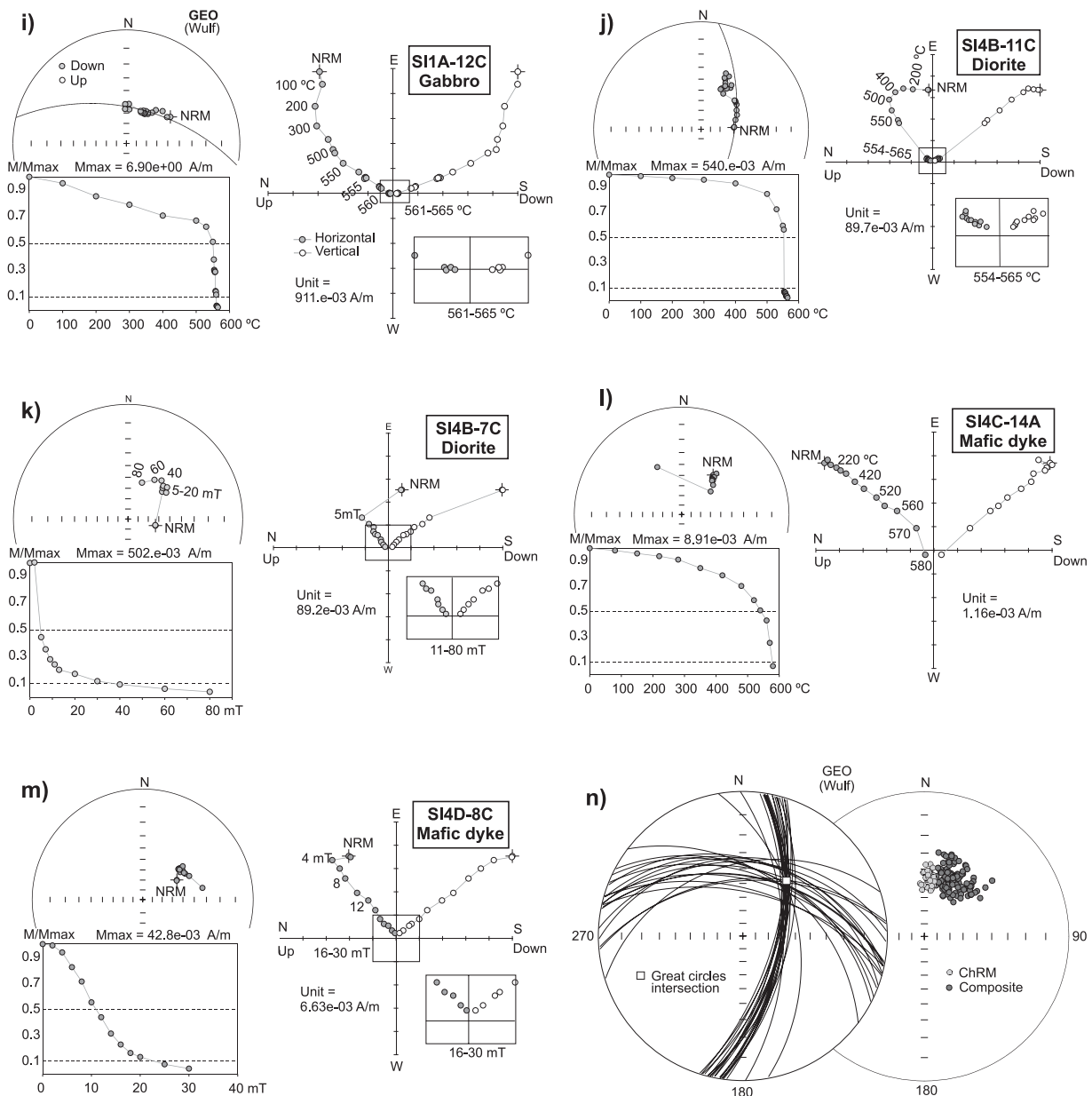


Figure 2. (Continued.)

the higher susceptibility values were obtained for the cooling curve; that could be related with the inversion of maghemite to magnetite at high temperatures (e.g. Dunlop & Özdemir 1997).

5.3 Hysteresis loops

The hysteresis loops are dominated by the paramagnetic (SI4D) or ferrimagnetic (SI1A) minerals or presented intermediate cases (Figs 3d–g). In all samples, a partial or total saturation appears around 0.1–0.3 T, indicating the presence of a moderate coercivity mineral.

The Day plot (Day *et al.* 1977), with standard boxes for single domain (SD), pseudo-single domain (PSD) and multidomain (MD), as redefined by Dunlop (2002) for titanomagnetites was used to infer the magnetic grain size. The values for remanence (J_{rs}/J_s) and coercivity (H_{cr}/H_c) ratios range from ~0.05 to 0.4 and from ~1.3 to 4.3, respectively (Fig. 3h). The distribution of these values

closely follows the envelope curves proposed by Dunlop (2002) for a mixture of SD and MD Ti-magnetite solid solution. That sustains the presence of stable SD palaeomagnetic recorders (e.g. Strangway *et al.* 1968; Davis & Evans 1976; Pariso & Johnson 1993; Dunlop & Özdemir 1997; Harrison & Putnis 1997).

6 PETROGRAPHY

To understand the origin and nature of magnetic minerals, we have conducted petrographic studies (transmitted and reflected light microscopy as well scanning electron microscopy—SEM) on gabbros (sites SI1A, SI5A and SI10A), diorites (site SI4B), mafic dykes (sites SI1B, SI4C and SI4D), Ca-metasediments (site SI3B) and subvolcanic breccia (SI2C).

The observed igneous samples (gabbros, diorites and micro-diorite dykes) reveal a preserved igneous texture although showing a variable degree of alteration products. Such effects are mostly

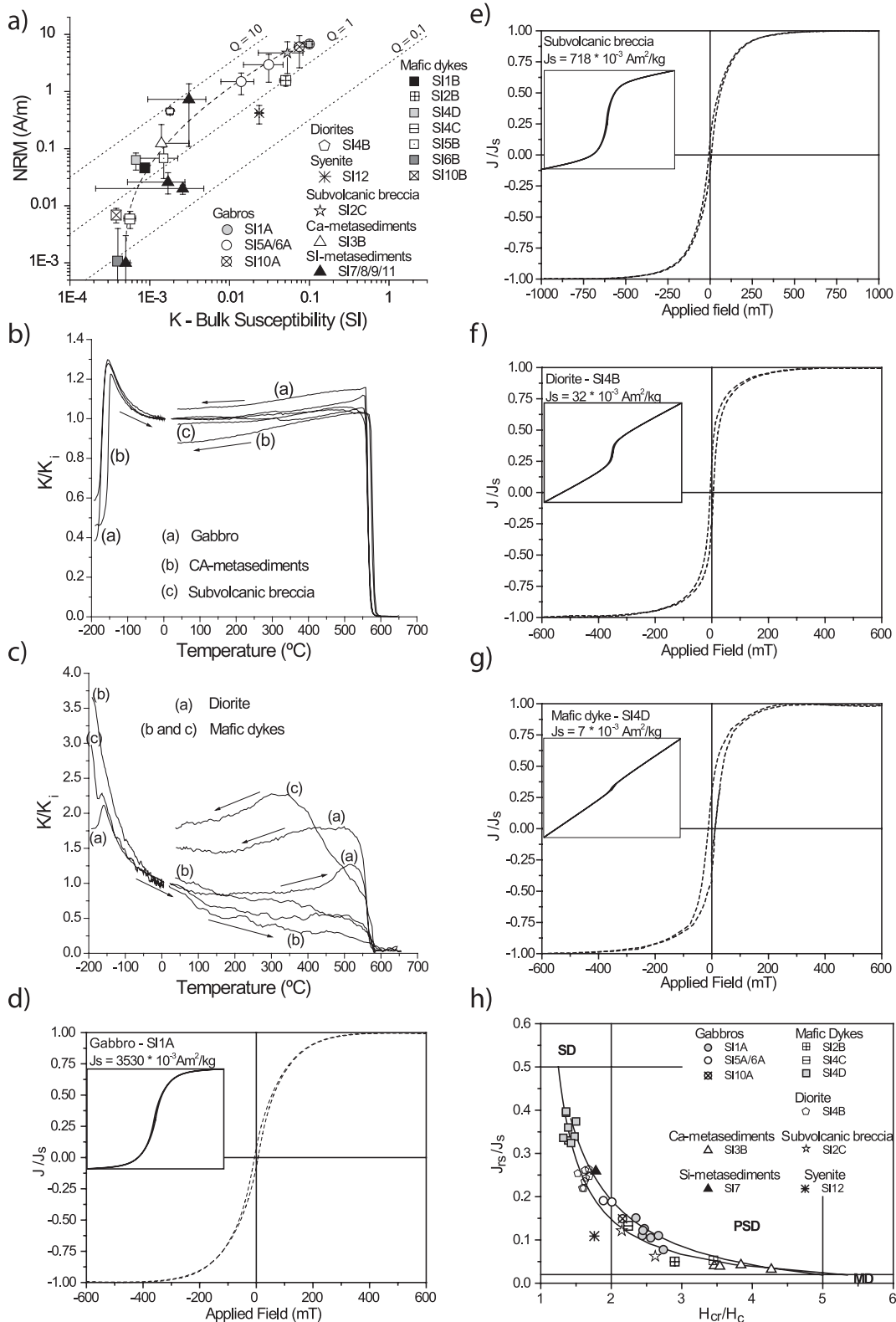


Figure 3. Representative rock magnetic results from the studied lithologies of the Sines massif. (a) Graph showing the variation of the bulk susceptibility (K) versus the NRM intensity (dotted lines indicate Koenigsberger ratio values of $Q = 0.1, 1$ and 10); (b) and c) thermomagnetic behaviour, with high temperature curves performed under Argon controlled atmosphere (values normalized by the room temperature susceptibility value); (d–g) representative hysteresis cycles after paramagnetic correction and normalized by the saturation magnetization J_s (inset displays hysteresis cycles before paramagnetic correction); (h) Day diagram (Day *et al.* 1977) with limits and mixing curves proposed by Dunlop (2002).

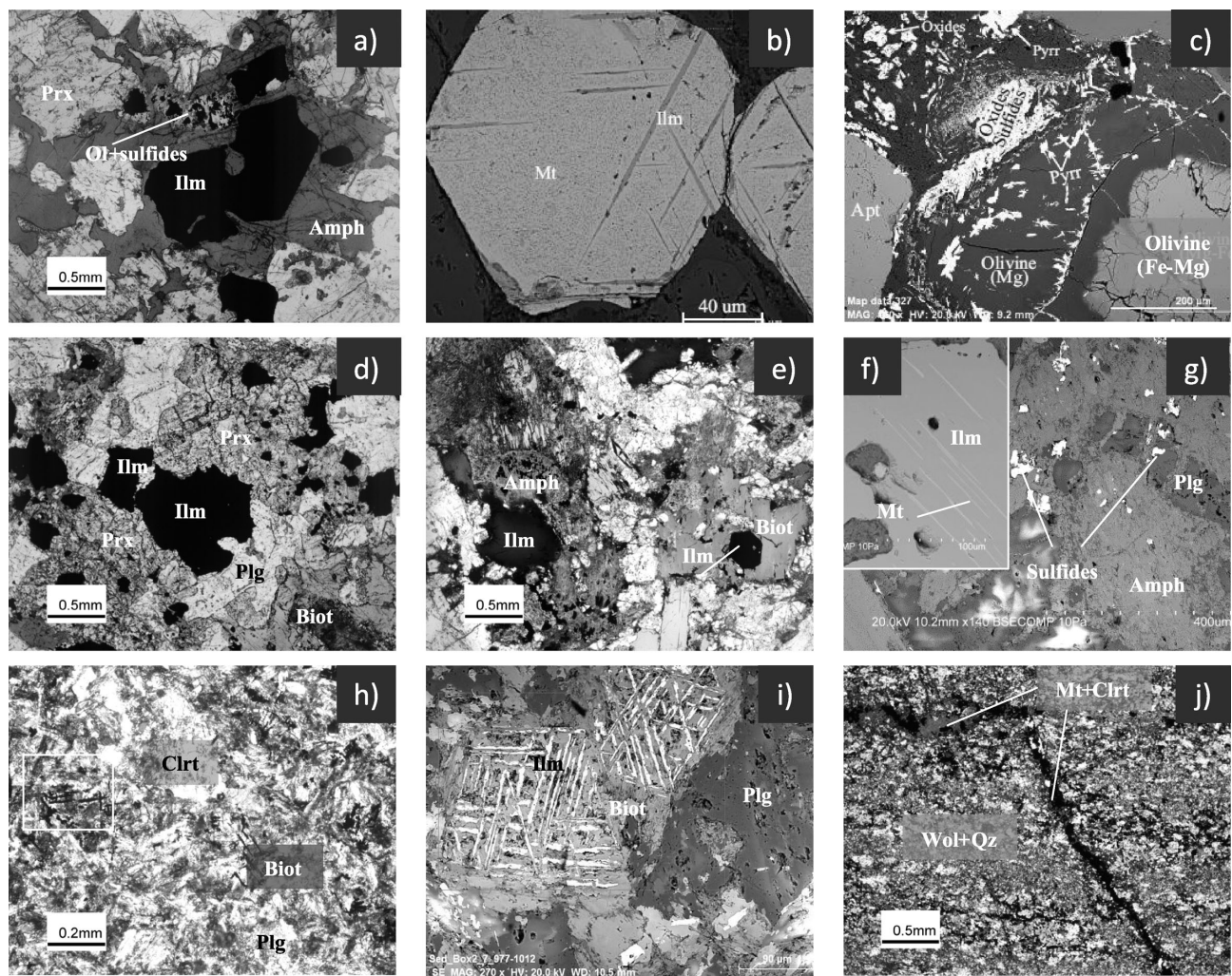


Figure 4. Textural relations of studied samples; petrographic (PT) and backscattered electron (BSE) images. (a) PT image of gabbro (sample SI-1) – ilmenite within amphibole and growth of oxides, and sulphides and phyllosilicates after olivine as consequence of low-temperature effects; (b) detail of gabbro (sample SI-1), BSE image of euhedral magnetites with exsolved thick lamellae of ilmenite; (c) detail of gabbro (sample SI-1), BSE image showing textural relations of magnetite, ilmenite and sulphides (pyrite/pyrrhotite) and apatite (Apt) in a silicate matrix; (d) PT image of subvolcanic breccia (sample SI-2C) with ilmenite associated with pyroxene; (e) PT image of diorite (sample SI4B) showing very retrogressed Fe-Mg silicates; (f) detail of diorite (sample SI4B), BSE images of exsolution magnetite lamellae within ilmenite; (g) detail of diorite (sample SI4B), BSE image of retrogradation of igneous amphibole associated with sulphides development; (h) PT image of mafic dyke (sample SI-1B) showing highly retrogressed igneous assemblage with a thin granularity and exsolution of oxides; (i) detail of mafic dyke (sample SI-1B) BSE image of corrosion of ilmenite exsolution; (j) PT image of calc-silicified metasediment (sample SI-3B) showing the growth of magnetite intimately associated with a latter vein with chlorite and magnetite. Abbreviations as Prx, pyroxene; Ol, olivine; Ilm, ilmenite; Amph, amphibole; Mt, magnetite; Apt, apatite; Plg, plagioclase; Biot, biotite; Wol, Wollastonite; Clrt, chlorite; Qz, quartz.

due to low-temperature hydrothermal/fluid–rock interactions with a progressive degree of secondary mineralogy growth, from gabbros and subvolcanic breccia to diorites and microdiorite dykes.

The gabbros clearly preserve the ferromagnesian phases (olivine, pyroxene, amphibole and biotite), plagioclase as well as primary ilmenite intimately associated with the amphibole (Fig. 4a). Less common ilmenite and magnetite occur as small grains or as small lamellae exsolutions within the former Ti-magnetite (Fig. 4b). Despite the well-preserved igneous assemblage of gabbro, some secondary minerals are present, mostly related with a partial replacement of olivine by an assemblage of secondary iron-sulphur, white mica and white amphibole (Fig. 4c). Biotite replacement by chlorite is occasionally observed.

The studied sample of subvolcanic breccia (SI2C) corresponds petrographically to the gabbro–dioritic rock. It is composed mainly of clinopyroxene (dominant mafic phase), biotite, amphibole,

plagioclase and opaque minerals (Fig. 4d). Pyroxene and amphibole appear associated with the fine-grained magnetite and larger ilmenite crystals. The igneous assemblage is slightly more altered than that of the gabbro and occasionally shows aggregates of the small-grained biotite, secondary amphibole and ilmenite, which apparently substitute the pyroxene. Small grains of ilmenite also occur associated with the later veins that cross the structure. The plagioclase is fresh with none or incipient sericitization.

In case of diorites, the main mafic minerals are amphibole and biotite (Fig. 4e), locally with clinopyroxene crystals. Ilmenite occurs as prismatic crystals inside biotite exhibiting magnetite exsolution lamellae (Fig. 4f). Although the primary igneous texture is essentially preserved, the degree of alteration is high, showing a widespread secondary overprint: (i) Biotite crystals show irregular contours/rims associated with the fine-grained magnetite and chlorite crystals reflecting a symplectitic texture; (ii) Amphibole

and pyroxenes are observable as relicts inside a secondary amphibole and associated sulphides that pseudo-morphous the igneous minerals (Figs 4e and g) and (iii) Plagioclases are highly fractured and show a moderate degree of sericitization. Such secondary mineral assemblages agree with late hydrothermal/fluid–rock interactions.

The mafic dykes samples correspond to microdiorites showing different texture types. The main igneous assemblage (biotite, amphibole and plagioclase) appears strongly modified by the conspicuous development of secondary mineralogy (sericite, calcite, amphibole and chlorite; Fig. 4h). Sericite occurs in appreciable amounts associated to plagioclase, whereas actinolite and chlorite associates mainly with primary amphibole replacing it almost entirely. The opaque minerals occur in minute amounts as small grains (ilmenite) as well as the largest opaque grains that correspond mainly to pyrite \pm chalcopyrite. Some corroded relicts of lamellae exsolutions of ilmenite associated with biotite (Fig. 4i) reflect the pervasive low-temperature event.

The metasediment at the northern contact (metalimestone—SI3B) exhibits a millimetre-to-centimetre-layered texture truncated by small orthogonal veins (Fig. 4j). The layered texture reflects differences in the grain size associated with wollastonite and opaque minerals (magnetite) crystallization. The magnetite growth is associated with the small veins filled with chlorite, reflecting a latter recrystallization of sediment associated with the emplacement of the Sines massif.

These petrographic analyses are a complement to the former descriptions done by Brak-Lamy (1951), Aires-Barros (1962) and Canilho (1972). The chemical analysis by microprobe (Canilho 1989) of opaque minerals of the main rock types of massif (gabbro, diorite and syenite) mostly revealed the presence of Ti-poor magnetite (with \sim 90 per cent of whole-Fe) and ilmenite (with \sim 50 per cent of TiO_2).

7 MAGNETIC FABRIC

Palaeomagnetic directions can be affected by a rock magnetic anisotropy when this anisotropy is very high (e.g. Jackson *et al.* 1991; Tauxe 2005; Borradaile & Almqvist 2008). AMS ellipsoids of samples from the Sines massif show low magnetic anisotropy (mostly with P' values lower than 1.08) without a preferential shape. The gabbros and diorites exhibit vertical NE–SW trending magnetic foliation (K_1 – K_2 plane). Well-clustered magnetic lineation (K_1) of gabbros plunges subvertically while for diorites are spread along the magnetic foliation plane with a clearly dominant vertical orientation (Figs 5a and b). Mafic dykes from the sites SI4C and SI4D show magnetic foliation subparallel to the dyke plane and subhorizontal magnetic lineation. The dyke SI4C reveals the evolution of bulk and anisotropy parameters along the cross-sections, showing a regular increase of K_M , a decrease of P' and a transition from oblate to prolate shapes from the margin towards the centre of the dyke (Fig. 5c). In the dyke SI4D, such correlations between magnetic parameters along cross-sections have not been observed.

In summary, P' values in Sines are low, and regarding the orientation of AMS ellipsoids, magnetic fabrics of gabbro and diorite display some similarities contrary to their distinct palaeomagnetic directions. Moreover, for dykes with different orientations and different AMS fabric, similar palaeomagnetic directions are retrieved. Therefore, the palaeomagnetic directions are not significantly affected in the Sines massif by the rock magnetic anisotropy.

8 DISCUSSION

The scattering of palaeomagnetic directions and/or their migration retrieved during stepwise demagnetizations (Fig. 2) highlights the superposition of remanence components with distinct directions, at least in some of the samples. Moreover, this scattering is correlated with K , NRM and J_s values, with higher magnetic values showing more northerly declinations (*cf.* Figs 3a and 6a and b). In addition, J_s values and magnetic grain size (as inferred from coercivity ratio) are positively correlated, which means that the larger grains are associated with the northerly directions (Fig. 6c). This pattern raises several issues that need to be understood, particularly, the type and nature of magnetic carriers and subsequent cooling history of the Sines massif on a broader context, that is, during the final stages of the Cretaceous magmatic activity along the southwestern margin of the Iberian Peninsula.

8.1 Thermal (TRM) and chemical (CRM) remanent magnetization acquisition

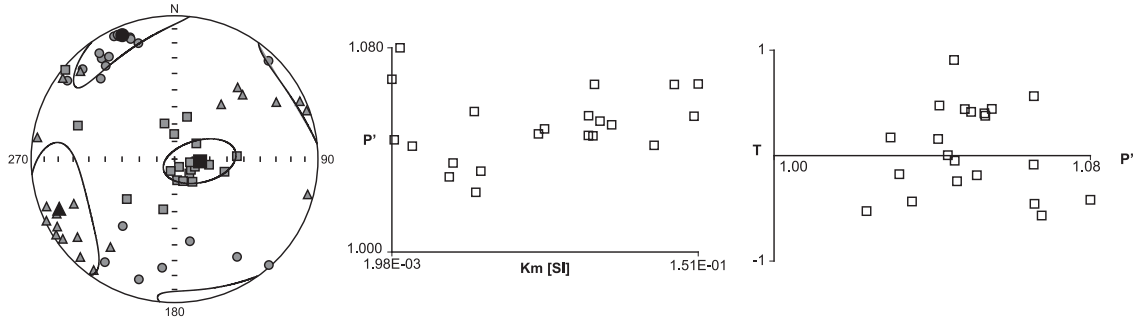
Magnetite is often coeval with the initial cooling stages of the igneous rocks for temperatures above 600 °C, but late magnetite occurrence is also frequent (e.g. Kamenov *et al.* 2003; Henry *et al.* 2012). In the Sines massif, magnetite occurs as isolated grains as well as composite ilmenite–magnetite grains that result from exsolution lamellae process of pre-existing Ti-spinels (e.g. Grommé *et al.* 1969; Perrin *et al.* 1991). Another family of magnetite is associated to the alteration of iron-rich silicates (e.g. olivine, pyroxene and biotite). This process is commonly contemporaneous with the initial cooling and can persist till temperatures around 550–400 °C (e.g. Brewster & O'Reilly 1988; Stakes *et al.* 1991), that is, below Curie temperature of magnetite. In metasediments, magnetite and pyrite result from iron-metasomatism and/or recrystallization (e.g. Silva *et al.* 2006a,b) thermally induced by the massif emplacement. For Sines, the coercivity and remanent ratios obtained by high field measurements give results that fit the envelop curves proposed by Dunlop (2002) for a mixture of SD and MD Ti-magnetite solid solution. That sustains the presence of stable small grains as palaeomagnetic recorders (e.g. Dunlop & Özdemir 1997; Harrison & Putnis 1997).

Although rocks from the Sines massif mostly preserve the original igneous assemblage and texture, they show evidences of low-temperature oxidation processes, which associated with hydrothermal/fluid–rock interactions, have variable effects on the primary mineralogy, including magnetite. These processes are slight to moderate in gabbros, subvolcanic breccias, metasediments and syenites, but pervasive in dykes (with exception of SI2B) and diorite.

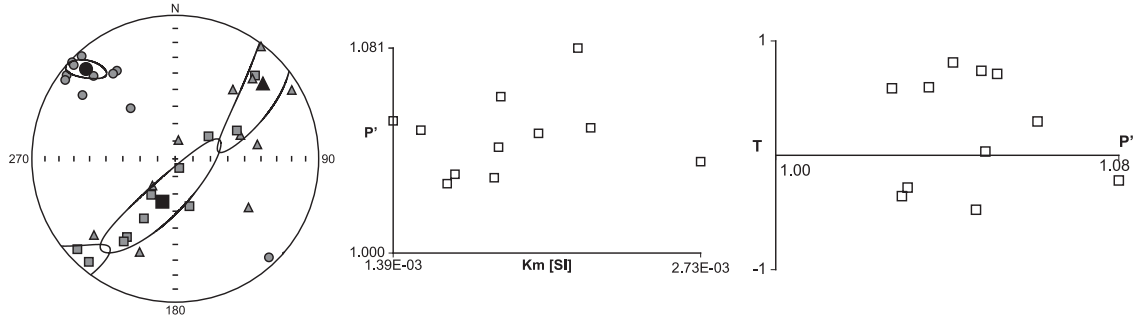
For the best preserved rocks, a total of 95 samples were analysed for palaeomagnetic purposes. From those, only 31 samples from seven sites (mentioned as P—primary component—, *cf.* Table 3) ensured the determination of a stable ChRM with mean, $3.9^\circ/46.5^\circ$ ($k = 209$ and $\alpha_{95} = 1.7^\circ$), mostly retrieved during the final thermal/AF demagnetization steps (typically above 550 °C/20 mT). They have the highest K , J_s and NRM values and also the largest grain size (PSD to small MD), which is coherent with the expected properties of a TRM for intrusive facies.

From the most altered rocks (a total of 96 analysed samples, most of them from dykes and diorite), palaeomagnetic analyses point for the presence of a composite NRM (mentioned as S—secondary component—, *cf.* Table 3), as evidenced by: (i) during demagnetization, the migration of directions along NNE- and

a) Gabros (Sites SI1A, SI5A, SI6A, SI10A)

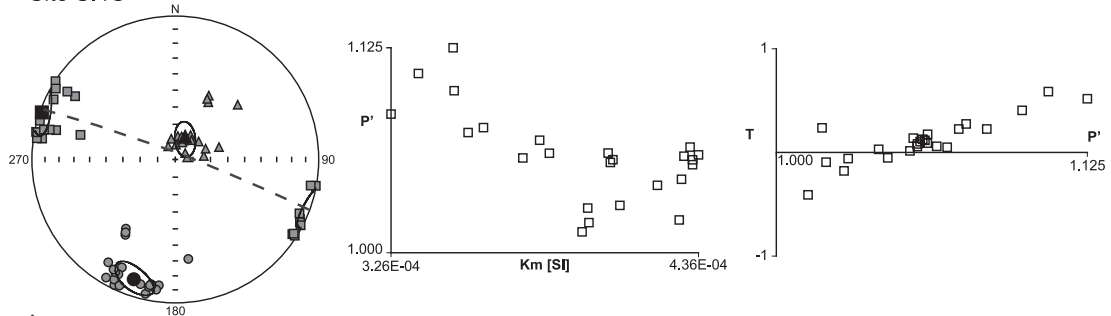


b) Diorites (Site SI4B)



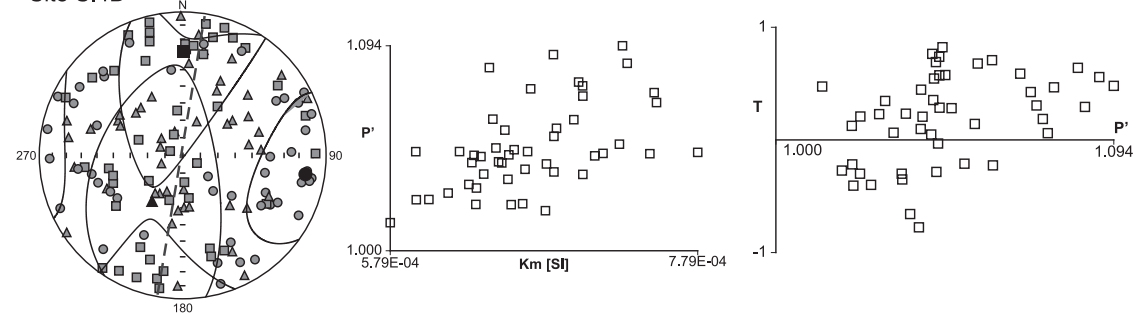
c) Mafic dykes

Site SI4C



Mafic Dyke (110°/85N; thickness = 80 cm)

Site SI4D



Mafic Dyke (190°/90; thickness = 110 cm)

Figure 5. AMS results for distinct type of rocks are presented. (Left-hand side) Stereographic projections (lower hemisphere) with indication of the maximum K_1 (squares), intermediate K_2 (triangles) and minimum K_3 (circles) magnetic susceptibility principal axes; (middle) corrected degree of anisotropy P' versus bulk magnetic susceptibility K_m ; and (right-hand side) P' versus the shape parameter T (Jelínek 1981).

ESE-dipping great circles; (ii) the scattering of palaeomagnetic declinations between $N15^\circ$ and $N50^\circ$, which corresponds to the more easterly declinations retrieved for the massif and (iii) the fitted lines (however, mostly corresponding to slightly curved lines) on the

Zijderveld diagram do not exactly cross the axes origin, that is, are not ChRMs.

This palaeomagnetic behaviour is observed for samples with the smaller grain sizes (corresponding to small PSD or large SD), that

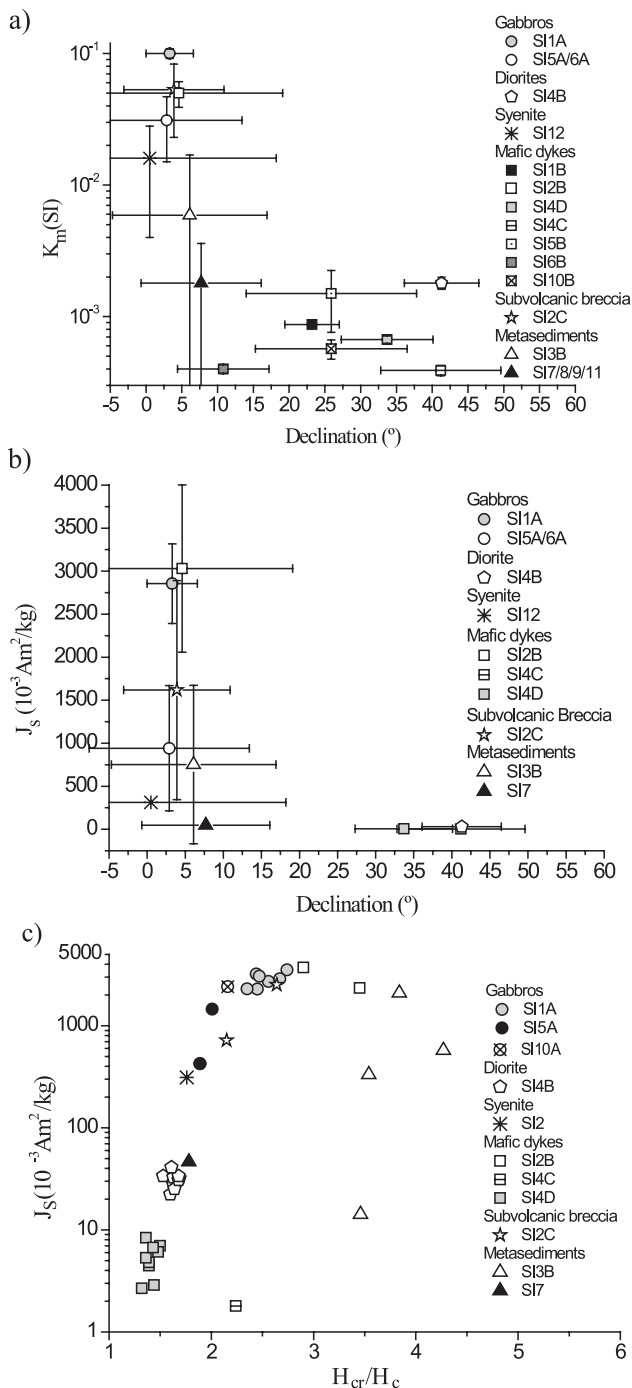


Figure 6. Plots showing for different sites/lithologies of the Sines massif the variation of main palaeomagnetic declinations with respect to the bulk magnetic susceptibility— K_m (a) and saturation magnetization— J_s (b); error bars correspond to declination error (Butler 1992) and standard deviation for K_m and J_s ; (c) plot showing the variation of coercivity ratio (H_{cr}/H_c) versus J_s .

is, the ones for which the most stable palaeomagnetic directions can be expected. The presence of such small grain sizes is however surprising because crystallization rate in such intrusive rocks is relatively slow. Moreover, the variation of magnetic grain sizes is positively correlated with the intensity of J_s values, with smallest grain sizes corresponding to uncommon low J_s values (as well for K , NRM and Q) for mafic rocks (e.g. Tarling & Hrouda 1993;

Borradaile & Henry 1997). Furthermore, rocks with the smallest magnetic grains show irreversible thermomagnetic curves and Verwey transitions of low amplitude or entirely vanished. Therefore, altogether, such results suggest a secondary phenomenon at the origin of the smallest magnetic grains size, must probably, intense low-temperature oxidation processes (maghemitization).

An intense maghemitization leads to an effective and substantial decrease of the original mineral grain size and/or to a complete replacement by secondary non-magnetic mineral phases. Such evolution is in close agreement with the magnetic results here obtained and elsewhere by several works (e.g. Irving *et al.* 1970; Bleil & Petersen 1983; Johnson & Pariso 1993; Özdemir *et al.* 1993; Dunlop & Özdemir 1997; Silva *et al.* 2008). According to petrographic analyses, maghemitization is associated with conspicuous evidences of intense hydrothermal alteration. The presence of secondary minerals such as chlorite, sericite, sphene and iron-sulphides, and the pervasive alteration of dyke pristine mineralogy argue for the presence of important metasomatic effects associated with low-temperature hydrothermal events (Wilson *et al.* 1968; Ade-Hall *et al.* 1971). The evolution of such effects can be associated with acquisition of a stable CRM (e.g. Henry *et al.* 2004).

If such alteration processes are contemporaneous of the final cooling stages of the igneous massif, the TRM and the CRM share a similar palaeomagnetic direction. Otherwise, when the CRM is related with latter hydrothermal episodes, the NRM could result from the superposition of palaeomagnetic components with distinct directions (e.g. Johnson & Merrill 1972; Nishitani & Kono 1982; Hagstrum & Johnson 1986; Kelso *et al.* 1991). If both magnetizations have similar blocking temperature spectra, the ‘magnetization component’ determined during demagnetization is actually composite. That should be the case for the scattered easterly directions, while the northerly ChRM should correspond to the single TRM.

8.2 Evidences for SW Iberia widespread partial remagnetization during Late Cretaceous

As verified earlier, the great majority of the samples show a composite NRM due to the acquisition of a CRM promoted by hydrothermal circulation. This CRM is responsible for the scattering of palaeomagnetic directions between 15 and 50° azimuths, with NE directions achieved for samples that show a higher degree of alteration (mostly dykes and diorite), that is, where hydrothermal circulation was more pervasive. This scattering share the plane defined by the NNE-dipping great circles suggesting that the secondary component is located somewhere along this circle east of the primary north declination and was acquired after Sines intrusion.

The recent geochronological results attribute an age of ~76 Ma to the Sines massif (Miranda *et al.* 2009; Grange *et al.* 2010), an age that coincides with the beginning of the second major impulse of magmatic activity, which ceased at approximately 70 Ma. This period is characterized by a wider distribution of magmatic activity along the southwestern margin of Iberia, particularly between Lisbon and Monchique (Miranda *et al.* 2009). Thus, the presence of a thermal anomaly associated with such magmatic activity along this geographical area is indisputable. The Monchique igneous massif is the most prominent expression of the magmatic activity at the end of the Cretaceous, at about 70 Ma (Miranda *et al.* 2009; Grange *et al.* 2010) during reversed polarity Chron C31 (Gradstein *et al.* 2004). Palaeomagnetic studies indicated the intrusion of the Monchique massif during a period of reversed polarity, with mean ChRM at ~180°/–40° (Van der Voo 1969; Storetvedt *et al.* 1990; *cf.* Table 4,

Table 3. Palaeomagnetic results with statistical parameters, showing the site-mean and overall mean directions (P—primary; S—secondary), and the mean poles and intersection of main families of remagnetization circles. The mean palaeomagnetic pole (based on the primary directions—P) is also presented; *N*, number; *D*, declination; *I*, inclination; α_{95} , confidence limit; *k*, precision parameter; PLon, pole longitude; PLat, pole latitude; A_{95} , confidence limit for pole; *K*, precision parameter for pole.

Rock/Sites	Component	<i>N</i>	<i>D</i> (°)	<i>I</i> (°)	α_{95} (°)	<i>k</i>
Gabbro						
SI1A	P	12	3.3	48.7	2.2	395
	S	11	22.1	49.2	1.9	575
SI5A + SI6A	P	4	2.9	47.7	7.2	166
	S	11	24.9	44.7	4.4	109
Subvolcanic Breccia						
SI2C	P	4	3.9	40.6	5.3	297
	S	7	23.4	33.5	6.7	82
Ca-Metasediments						
SI3B	P	3	6.1	45.0	7.7	258
	S	2	18.6	42.6	16.9	221
SI-Metasediments						
SI7 + SI8 + SI9 + SI11	P	4	7.7	49.4	5.7	257
	S	11	25.8	45.1	4.5	104
Syenite						
SI12	P	2	0.5	45.4	24.7	105
	S	2	18.4	36.1	34.3	55
Diorite						
SI4B	S	14	41.3	43.5	3.8	108
Mafic Dykes						
SI1B	S	12	23.3	40.9	2.9	222
SI2B	P	2	4.6	39.4	11.2	503
	S	5	16.3	33.3	5.7	181
SI4C	S	7	41.2	40.9	6.4	90
SI4D	S	16	33.7	40.0	4.9	57
SI5B	S	4	25.9	40.2	9.1	103
SI6B	S	3	10.8	43.7	4.6	478
SI10B	S	3	25.9	34.6	8.7	201
Overall Mean directions	P	31	3.9	46.5	1.8	209
	S	117	27.6	42.2	1.7	61
Great circles poles						
SI1A/SI2C/SI3B/SI4C/SI4D/SI5/SI6	NNE-dipping	18	191.9	48.4	4.7	55
SI4B/SI4C/SI4D	ESE-dipping	21	280.4	30.6	2.5	157
Great circles intersection		39	38.2	38.5	2.2	
Mean palaeomagnetic pole						
		<i>N</i>	PLong (°)	PLat (°)	A_{95} (°)	<i>K</i>
		31	332.0	-79.5	1.7	226

Table 4. Selected palaeomagnetic poles of Iberia for the uppermost Late Cretaceous (Campanian–Maastrichtian) and the resulting (by averaging) new pole (~83–70 Ma).

Site (locality)	Age (Ma)	Palaeomagnetic directions		Palaeomagnetic poles			Reference
		<i>D</i> (°)	<i>I</i> (°)	Long (°)	Lat (°)	A_{95} (°)	
Sintra complex	~83–80	359	43.5	354.5	-76.6	–	Van der Voo (1969)
Sines complex	~76	3.9	46.5	332.0	-79.5	1.7	This study
Monchique complex	~70	182	-37	344.9	-73.3	–	Van der Voo (1969)
		181	-42	347.4	-76.9	–	Storetvedt <i>et al.</i> (1990)
New palaeomagnetic pole for Iberia (~83–70 Ma)				345.4	-76.5	3.0	

Fig. 7a). The Monchique palaeomagnetic direction is intersected by the NNE-dipping plane that includes the ChRM and the main composite magnetization, suggesting that the hydrothermal activity responsible for the acquisition of the secondary component was

contemporaneous with the Monchique massif emplacement, that is, during the final stages of the second magmatic episode (Campanian/Maastrichtian period). However, since there is no evidence for the reverse polarity component in this study (Sines), a swing of

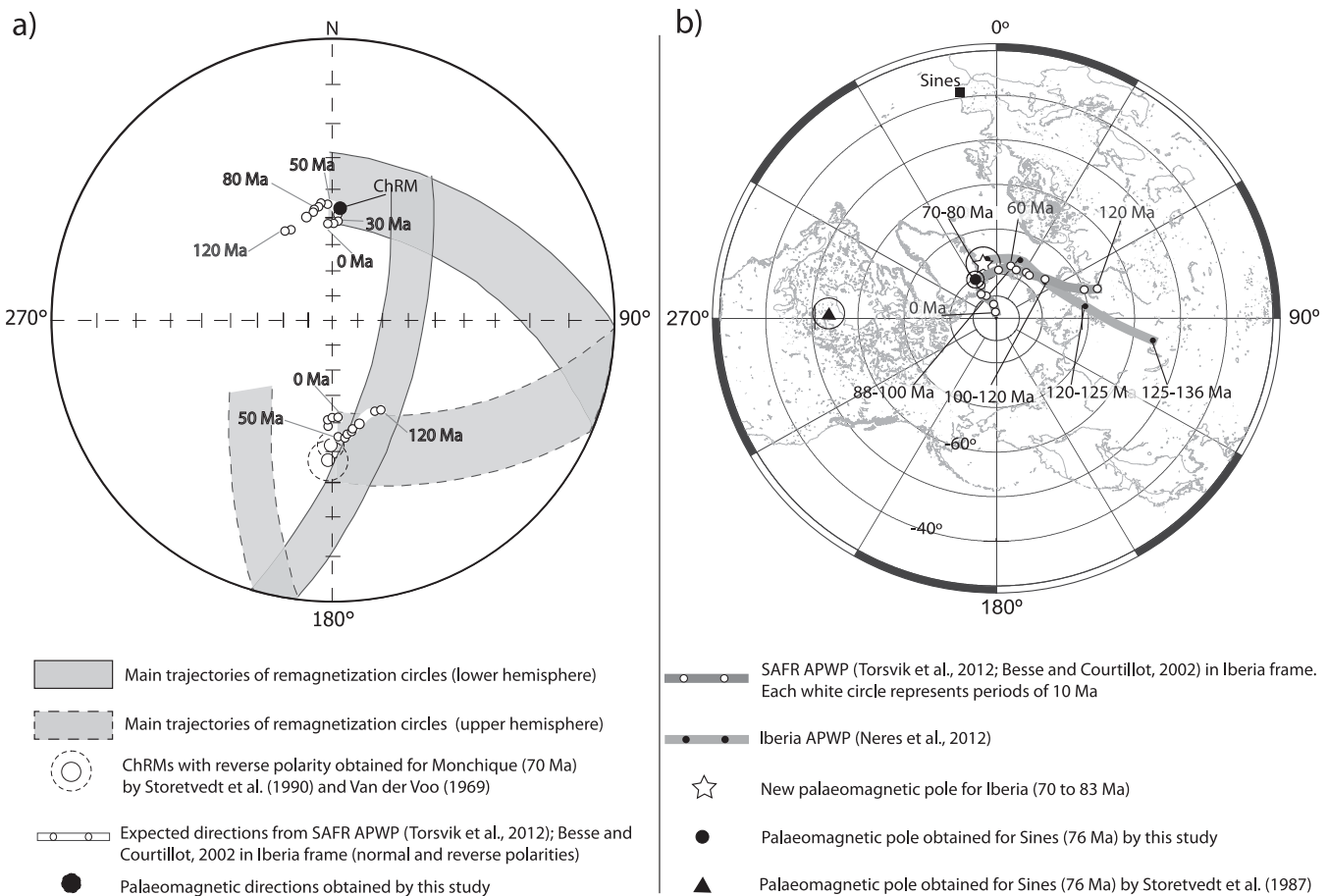


Figure 7. (a) Stereographic projection (lower hemisphere) of the ChRM direction and main trajectories of remagnetization circles for Sines (this study), and the expected directions from the southern Africa (SAFR) APWP (Besse & Courtillot 2002, 2003; Torsvik *et al.* 2012) (rotated for Iberia frame according to Finite Rotation Euler Poles defined by Neres *et al.* 2012 and Vissers & Meijer 2012); width of great circles belt corresponds to the α_{95} determined from the dispersion of great circles poles, following Fisher statistics; (b) Main palaeomagnetic poles for Sines and for Iberia with respective ages (stereographic projection in the Southern Hemisphere).

the Earth's magnetic field towards NE contemporaneous of the hydrothermal activity is another hypothesis that cannot be discarded. Indeed, polarity inversions are commonly preceded by geodynamo instabilities that promote significant deviations of palaeomagnetic directions (e.g. Chauvin *et al.* 1990; Clement 2000; Channell *et al.* 2004; Silva *et al.* 2012).

In what concerns the ESE-dipping great circles achieved at station S14 (Fig. 2, Table 3), it does not cross the apparent polar wander path (APWP) directions (Fig. 7a). However, it is not far from its reversed part (minimum angular difference about 25°). Without more constraints, it is difficult to have a reliable interpretation of its origin. Nonetheless, it cannot be related to a local tilting because the secondary component has been isolated using demagnetization analysis in the diorite yielding the ESE-dipping circles, and cannot be also related to a lightning effect because this should show up as a much higher NRM intensities and a wide variety of directions. Instead, this component may reflect the secular variation of the Earth's magnetic field (local component then acquired during a short duration event).

Evidences for partial remagnetizations are also found in several studies of palaeomagnetism performed in SW Iberia (e.g. Van der Voo 1969; Storetvedt *et al.* 1987, 1990; Galdeano *et al.* 1989; Márton *et al.* 2004; Neres *et al.* 2012). Thus, suggesting the presence of a regional thermal anomaly associated to the important

Late Cretaceous magmatism at north (Lisbon volcanic complex, ~ 72 Ma) and south (Monchique, ~ 70 Ma) of the Sines massif (~ 76 Ma).

8.3 A new palaeomagnetic pole for SW Iberia

Our results evidence the coexistence of a partially preserved primary magnetic mineralogy with hydrothermally altered magnetic phases. This clearly supports the occurrence of interactions between the cooling magmatic rocks and late hydrothermal circulation, which led to a composite NRM that include both the primary TRM and a secondary CRM. The primary and secondary directions are mainly included within the NNE-dipping great circles, with the most northerly directions associated with samples showing the lowest hydrothermal alteration, that is, a negligible effect of the CRM or even the absence of this CRM. These results, combined with the well-established fact of the northward migration of remanence directions, point to the northerly ChRM as the true primary magnetization of Sines.

Moreover, this ChRM is statistically coherent with the palaeomagnetic directions retrieved for the period squared between ~ 83 and 70 Ma (Table 4). For this period, four palaeomagnetic data have been selected in SW Iberia, two with normal polarity (Sines

and Sintra: mean direction $D = 1.4^\circ$, $I = 45.0^\circ$, with $k = 626$, $\alpha_{95} = 10.0^\circ$) and two with reversed polarity (Monchique: mean direction $D = 181.5^\circ$, $I = -39.5^\circ$, with $k = 513$ and $\alpha_{95} = 11.0^\circ$). The corresponding reversal test (McFadden & McElhinny 1990) results in an observed angle γ_O of 5.5° for a critical γ_c one of 9.6° . Therefore, these four palaeomagnetic data share the same direction, with a mean direction $D = 1.5^\circ$, $I = 42.3^\circ$, with $k = 366$ and $\alpha_{95} = 3.7^\circ$. For last, the associated palaeomagnetic pole (long. = 345.4° , lat. = -76.5° , for $N = 4$, with $K = 540$ and $A_{95} = 3.0^\circ$; cf. Fig. 7b) is not significantly different from the synthetic APWP of Iberia (Torsvik *et al.* 2012).

9 CONCLUSIONS

The palaeomagnetic analysis conducted on rocks from the Sines massif gave a ChRM with a northerly declination ($D = 3.9^\circ$, $I = 46.5^\circ$, with $k = 209$ and $\alpha_{95} = 1.7^\circ$, for $N = 31$) as the new reference for Sines. This direction (and its palaeomagnetic pole: long. = 332.0° , lat. = -79.5° , with $K = 226$ and $A_{95} = 1.7^\circ$) closely agrees with the palaeomagnetic data reported for the other subvolcanic (Sintra and Monchique) and volcanic (Lisbon) Late Cretaceous complexes (Tables 1 and 4). On the other hand, it contrasts with the mean direction of $D/I = 40.8^\circ/41.4^\circ$, interpreted for Sines by Storetvedt *et al.* (1987) as the primary magnetization, which actually corresponds to a composite magnetization, as shown here. Therefore, the kinematic model for Iberia with two rotations of opposite sense (Storetvedt *et al.* 1987, 1990) is definitely discarded. In addition, our new result for Sines corroborates the view that states that Iberia did not experience any significant clockwise rotation with respect to stable Europe in the uppermost Late Cretaceous (Campanian–Maastrichtian) (e.g. Van der Voo 1993).

For the period bracketed between ~ 83 and 70 Ma, four palaeomagnetic data have been selected in SW Iberia, two with normal polarity (Sines and Sintra) and two with reversed polarity (Monchique) (Table 4). These directions passed the reversal test (McFadden & McElhinny 1990) and form a reliable and well-defined palaeomagnetic mean direction ($D = 1.5^\circ$, $I = 42.3^\circ$ with $k = 366$ and $\alpha_{95} = 3.7^\circ$) for the Campanian period (~ 83 –70 Ma). The associated palaeomagnetic pole, defined by long = 345.4° , lat = -76.5° (with $K = 540$ and $A_{95} = 3.0^\circ$), should be then considered a new reference pole for Iberia.

ACKNOWLEDGEMENTS

The field work was partially supported by FCT (Fundação para a Ciência e a Tecnologia, Portugal) through AMSPROGRESS (PTDC/CTE-GIX/098696/2008) project. We are also very grateful to José Mirão and Pedro Madureira from Centro Hercules (Évora University, Portugal) for technical assistance and helpful discussions. We are also very thankful to the Editor Eduard Petrovský, and Reviewers Randy Enkin and Juan Villalain, who guided us in strong improving the paper.

REFERENCES

Ade-Hall, J.M., Palmer, H.C. & Hubbard, T.P., 1971. The magnetic and opaque petrological response of basalts to regional hydrothermal alteration, *Geophys. J. R. astr. Soc.*, **24**, 137–174.
 Aires-Barros, L., 1962. Sobre a petrologia do complexo eruptivo de Sines, *Bol. Soc. geol. Port.*, **15**, 1–46.
 Argand, E., 1924. La Tectonique de l'Asie, *Int. Geol. Cong. Session Rep.*, **13**, pp. 170–372.

Bernard-Griffiths, J.B., Gérard, G., Cornen, G., Azambre, B. & Macé, J., 1997. Continental lithospheric contribution to alkaline magmatism: isotopic (Nd, Sr, Pb) and geochemical (REE) evidence from Serra de Monchique and Mount Ormonde complexes, *J. Petrol.*, **38**, 115–132.
 Besse, J. & Courtillot, V., 2002. Apparent and true polar wander and the geometry of the geomagnetic field over the last 200 Myr, *J. geophys. Res.*, **107**(B11), 2300, doi:10.1029/2000JB000050.
 Besse, J. & Courtillot, V., 2003. Correction to 'Apparent and true polar wander and the geometry of the geomagnetic field over the last 200 Myr', *J. geophys. Res.*, **108**(B10), 2469, doi:10.1029/2003JB002684.
 Bleil, U. & Petersen, N., 1983. Variations in magnetization intensity and low-temperature titanomagnetite oxidation of ocean floor basalts, *Nature*, **301**, 384–388.
 Borradaile, G.J. & Almqvist, B.S., 2008. Correcting distorted paleosecular variation in late glacial lacustrine clay, *Phys. Earth planet. Inter.*, **166**, 30–43.
 Borradaile, G.J. & Henry, B., 1997. Tectonic applications of magnetic susceptibility and its anisotropy, *Earth Sci. Rev.*, **42**, 49–93.
 Borradaile, G.J. & Jackson, M., 2010. Structural geology, petrofabrics and magnetic fabrics (AMS, AARM, AIRM), *J. Struct. Geol.*, **32**, 1519–1551.
 Brak-Lamy, J.A.N., 1951. Primeira contribuição petroquímica relativa ao complexo eruptivo de Sines, *Comum. Serv. geol. Port.*, **32**, 131–144.
 Brewster, D. & O'Reilly, W., 1988. Magnetic properties of synthetic analogues of the altered olivines of igneous rocks, *Geophys. J. Int.*, **95**, 421–432.
 Bullard, E., Everett, J. & Smith, A.G., 1965. The fit of the Continents around the Atlantic, *Philos. Trans. R. Soc. Lond., A*, **258** (1088), 41–51.
 Butler, R.F., 1992. *Paleomagnetism: Magnetic Domains to Geologic Terrains*, Blackwell Scientific Publications, 319pp.
 Canilho, M.H., 1972. Estudo geológico-petrográfico do maciço eruptivo de Sines, *Bol. Mus. Lab. Min. FCUL*, **12**, 77–161.
 Canilho, M.H., 1989. Elementos de geoquímica das rochas do maciço de ígneo de Sines, *Ciências da Terra*, **10**, 65–80.
 Canilho, M.H. & Abranches, M.C., 1982. Rb-Sr geochronology of the Sines alkaline complex, *Comum. Serv. geol. Port.*, **68**, 237–240.
 Carey, S.W., 1958. A tectonic approach to continental drift, in *Symposium on Continental Drift*, Hobart, Tasmania, pp. 177–355.
 Carvalho, J.P.G., Torres, L.M. & Afilhado, A., 1998. Delimitação do maciço sub-vulcânico de Sines offshore a partir de dados geofísicos, *Comum. Serv. geol. Port.*, **84**, D57–D60.
 Channell, J.E.T., Curtis, J.H. & Flower, B.P., 2004. The Matuyama-Brunhes boundary interval (500–900 ka) in North Atlantic drift sediments, *Geophys. J. Int.*, **158**, 489–505.
 Chauvin, A., Roperch, P. & Duncan, R.A., 1990. Records of geomagnetic reversals from volcanic islands of French Polynesia 2. Paleomagnetic study of a flow sequence (1.2–0.6 Ma) from the island of Tahiti and discussion of reversal models, *J. geophys. Res.*, **95**, 2727–2752.
 Clement, B.M., 2000. Comment on the Lau Basin Cobb Mountain records by Abrahamsen and Sager, *Phys. Earth planet. Inter.*, **119**, 173–184.
 Davis, P.M. & Evans, M.E., 1976. Interacting single-domain properties of magnetite intergrowths, *J. geophys. Res.*, **81**, 989–994.
 Day, R., Fuller, M. & Schmidt, V.A., 1977. Hysteresis properties of titanomagnetites: grain size and composition dependence, *Phys. Earth planet. Inter.*, **13**, 260–267.
 Dinarés-Turell, J. & García-Senz, J., 2000. Remagnetization of Lower Cretaceous limestones from the southern Pyrenees and relation to the Iberian plate geodynamic evolution, *J. geophys. Res.*, **105**, 19 405–19 418.
 Dunlop, D.J., 2002. Theory and application of the Day plot (M_{TS}/M_S versus H_{cr}/H_c). 2. Application to data for rocks, sediments, and soils, *J. geophys. Res.*, **107**(B3), doi:10.1029/2001JB000487.
 Dunlop, D.J. & Özdemir, Ö., 1997. *Rock Magnetism: Fundamentals and Frontiers*, Cambridge Studies in Magnetism, Cambridge University Press, 573pp.
 Du Toit, A.L., 1937. *Our Wandering Continents*, Oliver & Boyd, 365pp.
 Ferreira, M.R.P. & Macedo, C.R., 1979. K-Ar ages of the Permian-Mesozoic basaltic activity in Portugal, Abstracts VI, in *Europ. Col. Geochron., Cosmochron. and Isotope Geology*, Norway, pp. 26–27.

- Fisher, R.A., 1953. Dispersion on a sphere, *Proc. R. Soc. Lond., A*, **217**, 295–305.
- Galdeano, A., Moreau, M.G., Pozzi, J.P., Berthou, P.Y. & Malod, J.A., 1989. New paleomagnetic results from Cretaceous sediments near Lisboa (Portugal) and implications for the rotation of Iberia, *Earth planet. Sci. Lett.*, **92**, 95–106.
- Girdler, R.W., 1965. Continental drift and the rotation of Spain, *Nature*, **207**, 396–398.
- Gong, Z., Langereis, C.G. & Mullender, T.A.T., 2008. The rotation of Iberia during the Aptian and the opening of the Bay of Biscay, *Earth planet. Sci. Lett.*, **273**, 80–93.
- Gradstein, F.M., Ogg, J.G. & Smith, A.G., 2004. A geologic time scale 2004, *Lethaia*, **37**, 175–181.
- Grange, M., Scharer, U., Merle, R., Jirardeau, J. & Cornen, G., 2010. Plume-lithosphere interaction during migration of Cretaceous alkaline magmatism in SW Portugal: evidence from U-Pb ages and Pb-Sr-Hf isotopes, *J. Petrol.*, **10**, 1–28.
- Grommé, C.S., Wright, T.L. & Peck, D.L., 1969. Magnetic properties and oxidation of iron-titanium oxide minerals in Alae and Makaopuhi lava lakes, Hawaii, *J. geophys. Res.*, **74**, 5277–5293.
- Hagstrum, J.T. & Johnson, C.M., 1986. A paleomagnetic and stable isotope study of the pluton at rio Hondo near Questa, New-Mexico: implications for CRM related to hydrothermal alteration, *Earth planet. Sci. Lett.*, **78**, 296–314.
- Harrison, R.J. & Putnis, A., 1997. Interaction between exsolution microstructures and magnetic properties of the magnetite-spinel solid solution, *Am. Mineral.*, **82**, 131–142.
- Henry, B., Merabet, N., Derder, M.E.M. & Bayou, B., 2004. Chemical remagnetizations in the Illizi Basin (Saharan Craton, Algeria), *Geophys. J. Int.*, **156**, 200–212.
- Henry, B., Naydenov, K., Dimov, D., Jordanova, D. & Jordanova, N., 2012. Relations between the emplacement and fabric-forming conditions of the Kapitan-Dimitriev pluton and the Maritsa shear zone (Central Bulgaria): magnetic and visible fabrics analysis, *Int. J. Earth Sci.*, **101**, 747–749.
- Hext, G., 1963. The estimation of second-order tensor, with related tests and designs, *Biometrika*, **50**, 353–357.
- Inverno, C., Manuppella, G., Zbyszewski, G., Pais, J. & Ribeiro, L., 1993. Notícia Explicativa da Folha 42-C Santiago do Cacém. Carta Geológica de Portugal de 1/50 000, Serviços Geológicos de Portugal, 75pp.
- Irving, E., Park, J.K., Haggerty, S.E., Aumento, F. & Loncarevic, B., 1970. Magnetism and opaque mineralogy of basalts from Mid-Atlantic Ridge at 45 degrees N, *Nature*, **228**(5275), 974–976.
- Jackson, M.J., Banerjee, S.K., Marvin, J.A., Lu, R. & Gruber, W., 1991. Detrital remanence, inclination errors, and anhysteretic remanence anisotropy: quantitative model and experimental results, *Geophys. J. Int.*, **104**, 95–103.
- Jelínek, V., 1978. Statistical processing of anisotropy of magnetic susceptibility measured on groups of specimens, *Stud. Geophys. Geod.*, **22**, 50–62.
- Jelínek, V., 1981. Characterization of the magnetic fabric of rocks, *Tectonophysics*, **79**, T63–T67.
- Johnson, H.P. & Merrill, R.T., 1972. Magnetic and mineralogical changes associated with low-temperature oxidation of magnetite, *J. geophys. Res.*, **77**(2), 334–341.
- Johnson, H.P. & Pariso, J.E., 1993. Variations in oceanic crustal magnetization—systematic changes in the last 160 million years, *J. geophys. Res.*, **98**, 435–445.
- Kamenov, B., von Quadt, A. & Peytcheva, I., 2003. Capitan-Dimitriev pluton in Central Srednogorie, Bulgaria: mineral chemistry, geochemistry and isotope evidence for magma-mixing origin, *Geochem. Mineral. Petrol.*, **40**, 21–53.
- Kelso, P.R., Banerjee, S.K. & Worm, H.U., 1991. The effect of low-temperature hydrothermal alteration on the remanent magnetization of synthetic titanomagnetites: a case of acquisition of chemical remanent magnetization, *J. geophys. Res.*, **96**, 19 545–19 553.
- Kirschvink, J.L., 1980. The least-squares line and plane and the analysis of palaeomagnetic data, *Geophys. J. R. astr. Soc.*, **62**, 699–718.
- Macintyre, R.M. & Berger, G.W., 1982. A note on the geochronology of the Iberian Alkaline Province, *Lithos*, **15**, 133–136.
- Márton, E., Abranches, M.C. & Pais, J., 2004. Iberia in the Cretaceous: new paleomagnetic results from Portugal, *J. Geodyn.*, **38**, 209–221.
- McFadden, P.L. & McElhinny, M.W., 1990. Classification of the reversal test in palaeomagnetism, *Geophys. J. Int.*, **103**, 725–729.
- Mendes, F., 1968. Contribution à l'étude géochronologique, par la méthode au strontium, des formations cristallines du Portugal, *Bol. Mus. Lab. Min. Geol.*, **11**, 1–150.
- Miranda, R., Valadares, V., Terrinha, P., Mata, J., Azevedo, M.R., Gaspar, M., Kullberg, J.C. & Ribeiro, C., 2009. Age constraints on the Late Cretaceous alkaline magmatism on the West Iberian margin, *Cretaceous Res.*, **30**, 575–586.
- Moreau, M.G., Canérot, J. & Malod, J.-A., 1992. Paleomagnetic study of Mesozoic sediments from the Iberian Chain (Spain): suggestions for Barremian remagnetization and implications for the rotation of Iberia, *Bull. Soc. geol. France*, **163**, 393–402.
- Moreau, M.G., Berthou, J.Y. & Malod, J.-A., 1997. New paleomagnetic Mesozoic data from the Algarve (Portugal): fast rotation of Iberia between the Hauterivian and the Aptian, *Earth planet. Sci. Lett.*, **146**, 689–701.
- Neres, M., Font, E., Miranda, J.M., Camps, P., Terrinha, P. & Mirão, J., 2012. Reconciling Cretaceous paleomagnetic and marine magnetic data for Iberia: new Iberian paleomagnetic poles, *J. geophys. Res.*, **117**, B06102, doi:10.1029/2011JB009067.
- Nishitani, T. & Kono, M., 1982. Grain size effects on the low-temperature oxidation of titanomagnetite, *J. Geophys.*, **50**, 137–142.
- Olivet, J.L., 1996. La Cinématique de la Plaque Ibérique, *Bull. Centres Rech. Explor. Prod. Elf Aquitaine*, **20**(1), 131–195.
- O'Reilly, W., 1984. *Rock and Mineral Magnetism*, Blackie, 220pp.
- Osete, M.L., Gómez, J.J., Pavón-Carrasco, J., Villalain, J.J., Palencia-Ortas, A., Ruiz-Martínez, V.C. & Heller, F., 2011. The evolution of Iberia during the Jurassic from palaeomagnetic data, *Tectonophysics*, **502**, 105–120.
- Özdemir, Ö., Dunlop, D.J. & Moskowitz, B.M., 1993. The effect of oxidation on the Verwey transition in magnetite, *Geophys. Res. Lett.*, **20**, 1671–1674.
- Pariso, J. & Johnson, H.P., 1993. Do lower crustal rocks record reversals of the Earth's magnetic field? magnetic petrology of oceanic gabbros from Ocean Drilling Program hole 735B, *J. geophys. Res.*, **98**, 16 013–16 032.
- Perrin, M., Prévot, M. & Mankinen, E., 1991. Low intensity of the geomagnetic field in Early Jurtassic time, *J. geophys. Res.*, **93**, 14 197–14 210.
- Petrovský, E. & Kapička, A., 2006. On determination of the Curie point from thermomagnetic curves, *J. geophys. Res.*, **111**, B12S27, doi:10.1029/2006JB004507.
- Ribeiro, A. et al., 1979. *Introduction à la géologie générale du Portugal*, Serviços Geológicos de Portugal, Lisboa, 114pp.
- Rock, N.M.S., 1982. The Late Cretaceous alkaline igneous province in the Iberian Peninsula, and its tectonic significance, *Lithos*, **15**, 111–131.
- Ruiz-Martínez, V.C., Torsvik, T.H., van Hinsbergen, D.J.J. & Gaina, C., 2012. Earth at 200 Ma: global palaeogeography refined from CAMP palaeomagnetic data, *Earth planet. Sci. Lett.*, **331–332**, 67–79.
- Schwarz, E.J., 1963. A paleomagnetic investigation of the Permo-Triassic red beds and andesites from the Spanish Pyrenees, *J. geophys. Res.*, **68**(10), 3265–3271.
- Sibuet, J.-C. & Collette, B.J., 1991. Triple junctions of the Bay of Biscay and North Atlantic: new constraints on the kinematic evolution, *Geology*, **19**, 522–525.
- Sibuet, J.-C., Srivastava, S.P. & Spakman, W., 2004. Pyrenean orogeny and plate kinematics, *J. geophys. Res.*, **109**, B08104, doi:10.1029/2003JB002514.
- Silva, P.F., Henry, B., Marques, F.O., Mateus, A., Madureira, P., Lourenço, N. & Miranda, J.M., 2006a. Variation of magnetic properties in sedimentary rocks hosting the Foum Zguid dyke (Southern Morocco): combined effects of re-crystallization and Fe-metasomatism, *Earth planet. Sci. Lett.*, **241**(3–4), 978–992.
- Silva, P.F., Henry, B., Marques, F.O., Madureira, P. & Miranda, J.M., 2006b. Paleomagnetic study of the Great Foum Zguid dyke (Southern Morocco): a positive contact test related to metasomatic processes, *Geophys. Res. Lett.*, **33**(21), L21301, doi:10.1029/2006GL027498.

- Silva, P.F. *et al.*, 2008. Magma flow, exsolution processes and rock metasomatism in the Great Messejana-Plasencia dyke (Iberian Peninsula), *Geophys. J. Int.*, **175**, 806–824.
- Silva, P.F., Henry, B., Marques, F.O., Hildenbrand, A., Madureira, P., Mériaux, C. & Kratinová, Z., 2012. Palaeomagnetic study of a sub-aerial volcanic ridge (São Jorge Island, Azores) for the past 1.3 Myr: evidence for the Cobb Mountain Subchron, volcano flank instability and tectono-magmatic implications, *Geophys. J. Int.*, **188**(3), 959–978.
- Srivastava, S.P., Roest, E.R., Kovacs, L.C., Oakey, G., Lévesque, S., Verhoef, J. & Macnab, R., 1990. Motion of Iberia since the Late Jurassic: results from detailed aeromagnetic measurements in the Newfoundland Basin, *Tectonophysics*, **184**, 229–260.
- Srivastava, S.P., Sibuet, J.C., Cande, S., Roest, W.R. & Reid, I.D., 2000. Magnetic evidence for slow seafloor spreading during the formation of the Newfoundland and Iberian margins, *Earth planet. Sci. Lett.*, **182**, 61–76.
- Stakes, D., Mével, C., Cannat, M. & Chaput, T., 1991. Metamorphic stratigraphy of Hole 735B, in *Proc. ODP, Sci. Results*, Vol. 118, eds Von Herzen, R.P., Fox, J., Palmer-Julson, A. & Robinson, P.T., College Station, TX (Ocean Drilling Program), pp. 153–180.
- Storetvedt, K.M., 1973. The rotation of Iberia: Caenozoic palaeomagnetism from Portugal, *Tectonophysics*, **17**, 23–39.
- Storetvedt, K.M., Mogstad, H., Abranches, M.C., Mitchell, J.C. & Serralheiro, A., 1987. Paleomagnetism and isotopic age data from Upper Cretaceous igneous rocks of W. Portugal: geological correlation and plate tectonic aspects, *Geophys. J. R. astr. Soc.*, **88**, 241–163.
- Storetvedt, K.M., Mitchell, J.C., Abranches, M.C. & Oftedahl, S., 1990. A new kinematic model for Iberia: further palaeomagnetic and isotopic age evidence, *Phys. Earth planet. Inter.*, **62**, 109–125.
- Strangway, D.W., Larson, E.E. & Goldstein, M., 1968. A possible cause of high magnetic stability in volcanic rocks, *J. geophys. Res.*, **73**, 3787–3796.
- Tarling, D.H. & Hrouda, F., 1993. *The Magnetic Anisotropy of Rocks*, Chapman & Hall, 217pp.
- Tauxe, L., 2005. Inclination shallowing and the geocentric axial dipole hypothesis, *Earth planet. Sci. Lett.*, **233**, 247–261.
- Teixeira, C., 1962. La structure annulaire subvolcanique des massifs éruptifs de Sintra, Sines et Monchique, *Est. Cient. of Prof. Carrington da Costa*, J. I. U., Lisboa, pp. 461–493.
- Torsvik, T.H. *et al.*, 2012. Phanerozoic polar wander, palaeogeography and dynamics, *Earth-Sci. Rev.*, **114**, 325–368.
- Van der Voo, R., 1967. The rotation of Spain: palaeomagnetic evidence from the Spanish Meseta, *Palaeogeog. Palaeoclimat. Palaeoecol.*, **3**, 393–416.
- Van der Voo, R., 1969. Paleomagnetic evidence for the rotation of the Iberian Peninsula, *Tectonophysics*, **7**, 5–56.
- Van der Voo, R., 1993. *Paleomagnetism of the Atlantic, Tethys and Iapetus Oceans*, Cambridge University Press, 411pp.
- Van der Voo, R. & Zijdeveld, J.D.A., 1971. Renewed paleomagnetic study of the Lisbon volcanics and implications for the rotation of the Iberian Peninsula, *J. geophys. Res.*, **76**, 3913–3921.
- Vandenbergh, J., 1980. New palaeomagnetic data from the Iberian Peninsula, *Geol. Mijnb.*, **59**, 49–60.
- Van Dongen, P.G., 1967. The rotation of Spain: palaeomagnetic evidence from the Eastern Pyrenees, *Palaeogeog. Palaeoclimat. Palaeoecol.*, **3**, 417–432.
- Verwey, E.J., 1939. Electronic conduction of magnetite (Fe₃O₄) and its transition point at low temperature, *Nature*, **144**, 327–328.
- Vissers, R.L.M. & Meijer, P.Th., 2012. Mesozoic rotation of Iberia: subduction in the Pyrenees? *Earth-Sci. Rev.*, **110**, 93–110.
- Watkins, N.D. & Richardson, A., 1968. Palaeomagnetism of the Lisbon volcanics, *Geophys. J. R. astr. Soc.*, **15**, 287–304.
- Williams, C.A., 1975. Sea-floor spreading in the Bay of Biscay and its relationship to the North Atlantic, *Earth planet. Sci. Lett.*, **24**, 440–456.
- Wilson, R.I., Haggerty, S.E. & Watkins, N.D., 1968. Variation of paleomagnetic stability and other parameters in a vertical traverse of a single Icelandic lava, *Geophys. J. R. astr. Soc.*, **16**, 79–96.
- Zbyszewski, G., 1941. Contribution à l'étude des terrains éruptifs du Cap Sines, *Comum. Serv. geol. Port.*, **22**, 85–98.